

Growth and disruption in the Lyra complex

S. Clavico^{1,2}, S. De Grandi¹, S. Ghizzardi³, M. Rossetti³, S. Molendi³, F. Gastaldello³, M. Girardi^{4,5}, W. Boschin^{6,7}, A. Botteon^{8,9,10}, R. Cassano⁹, M. Brüggen¹¹, G. Brunetti⁹, D. Dallacasa^{8,9}, D. Eckert¹², S. Ettori^{13,14}, M. Gaspari¹⁵, M. Sereno¹⁴, T. Shimwell^{10,16} and R. J. van Weeren¹⁰.

¹ INAF - Osservatorio Astronomico di Brera, via E. Bianchi 46, 23807 Merate, Italy

e-mail: sara.clavico@inaf.it, sabrina.degrandi@inaf.it

² Università degli Studi di Milano-Bicocca, Piazza della Scienza, 3, I-20126 Milano, Italy

³ INAF - IASF-Milano, Via E. Bassini 15, I-20133 Milano, Italy

⁴ Dipartimento di Fisica dell'Università degli Studi di Trieste, Italy

⁵ INAF - Osservatorio Astronomico di Trieste, via Tiepolo 11, I-34143 Trieste, Italy

⁶ Fundación Galileo Galilei - INAF (Telescopio Nazionale Galileo), Rambla José Ana Fernández Perez 7, E-38712 Breña Baja (La Palma), Canary Islands, Spain

⁷ Instituto de Astrofísica de Canarias, C/Vía Láctea s/n, E-38205 La Laguna (Tenerife), Canary Islands, Spain

⁸ Dipartimento di Fisica e Astronomia, Università di Bologna, via P. Gobetti 93/2, I-40129 Bologna, Italy

⁹ INAF - IRA, via P. Gobetti 101, I-40129 Bologna, Italy

¹⁰ Leiden Observatory, Leiden University, PO Box 9513, NL-2300 RA Leiden, The Netherlands

¹¹ Hamburger Sternwarte, Universität Hamburg, Gojenbergsweg 112, D-21029 Hamburg, Germany

¹² Department of Astronomy, University of Geneva, ch. d'Ecogia 16, 1290 Versoix, Switzerland

¹³ INAF, Osservatorio di Astrofisica e Scienza dello Spazio, via Pietro Gobetti 93/3, I-40129 Bologna, Italy

¹⁴ INFN, Sezione di Bologna, viale Berti Pichat 6/2, I-40127 Bologna, Italy

¹⁵ Department of Astrophysical Sciences, Princeton University, 4 Ivy Lane, Princeton, NJ 08544-1001, USA - Lyman Spitzer Jr. Fellow

¹⁶ ASTRON, the Netherlands Institute for Radio Astronomy, Postbus 2, NL-7990 AA Dwingeloo, The Netherlands

August 7, 2019

ABSTRACT

Context. Nearby clusters of galaxies, $z \lesssim 0.1$, are cosmic structures still under formation. Understanding the thermodynamic properties of merging clusters can provide crucial information on how they grow in the local universe.

Aims. A detailed study of the intra-cluster medium (ICM) properties of un-relaxed systems is essential to understand the fate of in-falling structures and, more generally the virialization process.

Methods. We analyzed a mosaic of XMM-Newton observations (240 ks) of the Lyra system ($z \sim 0.067$), that shows a complex dynamical state.

Results. We found that the main cluster RXC J1825.3+3026 is in a late merger phase, whereas its companion CIZA J1824.1+3029 is a relaxed cool-core cluster, we estimated for the pair a mass ratio of $\sim 1 : 2$. No diffuse X-ray emission is found in the region between them, indicating that these clusters are in a pre-merger phase. We found evidences of a galaxy group infalling on RXC J1825.3+3026 in an advanced state of disruption. The Southern Galaxy, one of the brightest galaxies in the Lyra complex, was very likely at the center of the infalling group. This galaxy has a gaseous "corona" indicating that it was able to retain some of its gas after the ram-pressure stripping of the intra-group medium. In this scenario the diffuse emission excess observed South-West of RXC J1825.3+3026 could be due to gas once belonging to the group and/or to cluster ICM dislocated by the passage of the group. Finally we identified three high velocity galaxies aligned between RXC J1825.3+3026 and the Southern Galaxy, two of these show evidences of gas stripped from them during infall. We estimate they are currently falling onto the main cluster with infall velocity of ~ 3000 km/s.

Conclusions. Our study of the Lyra complex provides important clues on the processes presiding over the virialization of massive clusters in the local Universe.

Key words. X-rays: galaxies: clusters: individual: RXC J1825.3+3026 – galaxies: clusters: individual: CIZA J1824.1+3029 – Galaxies: clusters: general – Galaxies: clusters: intracluster medium

1. Introduction

The currently favoured cosmological model predicts that structure formation proceeds hierarchically with the more massive dark matter halos growing through accretion of smaller halos, driven by gravity. Galaxy clusters are the most massive gravitationally bound objects which can be found at the present epoch and they have been forming

relatively recently, doubling their mass on average since $z \sim 0.5$ (Boylan-Kolchin et al. 2009; Gao et al. 2012). They are formed at the nodes of the filamentary network which constitutes the cosmic web, as the structure of the Universe on the largest scales is described in the Λ CDM model (for a review see Kravtsov & Borgani 2012).

If major mergers of equal size halos can be the most spectacular and energetic events since the Big Bang and leave substantial imprints on the observational appearance of clusters, they are rare events (e.g. Berrier et al. 2009; McGee et al. 2009; Fakhouri et al. 2010). A continuous and more gentle accretion of group-scale systems is the other important contributor to the growth of clusters. Observations show that the accretion of group-size systems is responsible at least of half of the accreted cluster mass from $z \sim 0.2$ to the present day, whereas the other half is likely to derive from smooth accretion of unbound matter within halos (e.g. Haines et al. 2018). Recent mergers leave their imprint on the distribution of the intra-cluster medium (ICM), which constitutes most of the baryonic mass of clusters and emits via bremsstrahlung in the soft X-ray band. Indeed, X-ray observations find that a high fraction ($> 40\%$) of clusters in representative sample of the nearby Universe ($z < 0.5$) displays clear disturbance (e.g. Rossetti et al. 2016; Lovisari et al. 2017).

Large-scale cosmological hydrodynamic simulations show that an important region for studying the mechanisms of growth of substructures in clusters is found between their R_{500} and R_{200} (e.g. Walker et al. 2019). In fact, in this region it is possible to observe the connections of the cosmic filaments with the innermost and already virialized part of the cluster (e.g., Eckert et al. 2015).

In addition to information on the mass growth of clusters, the study of accreting sub-structures at large radii gives the opportunity to study the physical properties of the ICM in the outskirts. During the infall of groups in clusters, the ram pressure applied by the ambient ICM is responsible for stripping their gas and heating it up, leading to the virialization of the gas in the main dark-matter halo. The dynamical scales involved in this process indicate that the thermal conductivity of the gas must be highly suppressed at these large distances from the cluster core (e.g., Eckert et al. 2014, 2017b; De Grandi et al. 2016).

In this work, we study the very special case of a system showing several substructures with different dynamical state (both pre- and post-merging) and different mass scales, at about R_{500} of the main cluster. This is the Lyra complex formed by the galaxy clusters pair RXC J1825.3+3026 and CIZA J1824.1 + 3029 (Fig. 1). RXC J1825.3+3026 (RXCJ1825 hereafter) was discovered by ROSAT in the X-rays ($z = 0.065$, Ebeling et al. 2002). Because of its relatively low galactic latitude, $b = 18.5$ degrees, it has been almost ignored until recently, when it was found to be one of the strongest ($\text{SNR} > 12$) sources of Sunyaev-Zeldovich (SZ) signal in the Planck all-sky cluster survey (Planck Collaboration et al. 2014) and became part of the XMM-Newton Cluster Outskirts Project (XCOP), an SZ-selected sample of 13 massive clusters observed in the X-rays by XMM-Newton up to the virial radius (Eckert et al. 2017a). RXCJ1825 is a massive cluster with a total mass $\sim 6 \times 10^{14} M_{\odot}$ within R_{200} (Ettori et al. 2019), and an irregular West-East X-ray morphology that suggests an un-relaxed dynamical status. Interestingly, its X-ray morphology shows also a clear extension to the South-West culminating on a bright elliptical galaxy (called the Southern Galaxy or SG in the rest of the paper). At ~ 16 arcmin North-West of RXCJ1825, there is

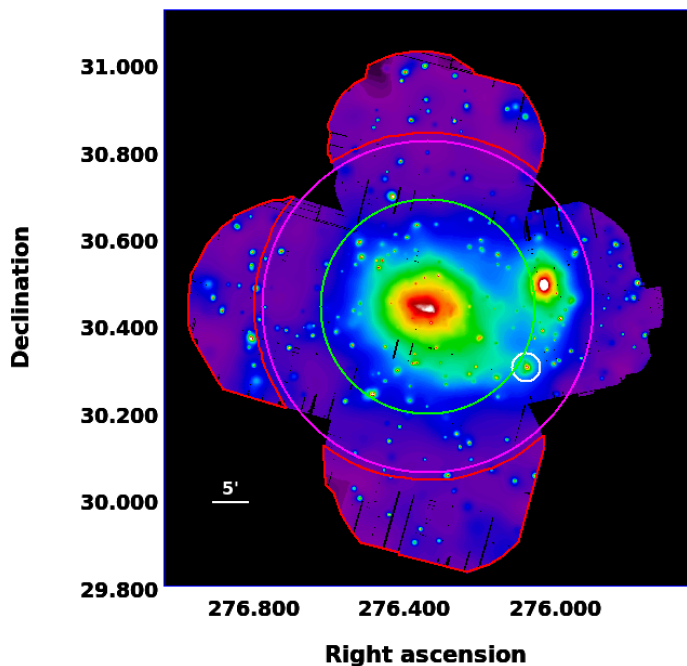


Fig. 1. XMM-Newton mosaic image of the Lyra cluster complex in units of counts pixel^{-1} in the $[0.7\text{--}1.2]$ keV energy band. The cluster RXCJ1825 is in the center of the image with the green and magenta circles representing the location of its R_{500} and R_{200} , respectively. The cluster CIZAJ1824 is West of RXCJ1825, whereas the white circle is centered on the Southern Galaxy. The image is corrected for the particle background (NXB). The red regions are the ones chosen for the estimate of the local sky background (see Sect. 2).

another smaller cluster: CIZA J1824.1 + 3029 (also known as NPM1G+30.0, and named CIZAJ1824 hereafter). Unlike RXCJ1825, CIZAJ1824 appears very regular in the X-rays.

The only optical observation available in the literature for this cluster is the redshift of its brightest cluster galaxy (BCG) $z = 0.072$ (Kocevski et al. 2007). Recently, Girardi et al. (2019) presented spectroscopic observation of the Lyra complex confirming that the two clusters and the Southern Galaxy are very close in the redshifts space and form a gravitationally bound system. Their new estimates for the redshifts of RXCJ1825 and CIZAJ1824 are $z = 0.0645$ and $z = 0.0708$, respectively. Here we focus our study on the analysis of the X-COP XMM-Newton mosaic centered on RXCJ1825 (240 ks in total) to determine the thermodynamic properties and the dynamic state of the whole Lyra system.

This paper is structured as follows: in Sect. 2 we describe our XMM-Newton mosaic observations together with their respective data reduction, imaging (Sect. 2.1), and spectral analysis (Sect. 2.2) techniques. In Sect. 3, we report the results for the whole Lyra system obtained from our data analysis, first focusing on its X-ray surface brightness features (Sect. 3.1), then on the thermodynamic profiles of the two clusters RXCJ1825 and CIZAJ1824 (Sect. 3.2), and finally on the 2D analysis of the spectral properties of several interesting regions (Sect. 3.3). In Sect. 4, we interpret and discuss our results. We summarize our main results in Sect. 5.

Throughout the paper, we assume a Λ CDM cosmology with $H_0 = 70 \text{ km s}^{-1}$, $\Omega_m = 0.3$ and $\Omega_{\Lambda} = 0.7$. At the redshift of the Lyra complex, $z = 0.067$ (Girardi et al. 2019),

¹ For a given over-density Δ , R_{Δ} is the radius for which $M_{\Delta}/(4/3\pi R_{\Delta}^3) = \Delta \rho_c$.

Table 1. XMM-Newton observations of the Lyra complex (RXCJ1825-CIZA1824) complex: field name, archival observation identification number, pointing position, total nominal exposure time and effective exposure time after soft-protons cleaning of the three EPIC detectors and ratio of the events IN and OUT of the MOS1 field of view.

Pointing	Obs.ID.	RA DEC (J2000) [deg]	Nominal [ksec]	MOS1 [ksec]	MOS2 [ksec]	<i>pn</i> [ksec]	IN/OUT
Center1	0744413501	276.3450, +30.4422	52.0	47.3	47.6	34.4	1.265
Center2	0744414101	276.3450, +30.4422	32.9	20.6	21.7	9.4	2.568
East	0744413901	276.7014, +30.4422	44.3	31.7	32.0	14.2	1.307
North	0744413601	276.3385, +30.7921	32.3	19.7	19.9	12.4	1.273
West	0744413701	275.9885, +30.4422	43.9	40.9	40.3	31.7	1.130
South	0744414801	276.3385, +30.0923	34.6	25.1	29.2	10.8	1.291

1 arcmin corresponds to ~ 77.5 kpc. Metal abundances are in units of $[X/H]$ normalized by the solar abundances of [Asplund et al. \(2009\)](#). All the quoted errors hereafter are at the 1σ confidence level.

2. Observations and Data Reduction

The Lyra complex was observed by XMM-Newton in 2014 with a mosaic of two central and four offset pointings. We did not consider one of the two central observations (Obs.ID. 0744414101) as we found that it was highly contaminated by quiescent soft protons (see Sect. [2.2](#)).

Table [1](#) contains information regarding the observations, such as the observation ID, the total and clean exposure times (after applying the ESAS tasks *mos-filter* and *pn-filter*) and the level of soft protons contamination obtained by comparing the measured count rate in a hard spectral band (10 – 12 keV) in the exposed and unexposed part of the field of view (IN/OUT, [Leccardi & Molendi 2008](#)). The analysis of the 5 remaining observations allowed us to explore the entire azimuth of the cluster out to $\sim R_{500}$ and its close companion CIZA1824. The data were processed using the XMM-Newton Scientific Analysis System (XMM-SAS) v.16.1.

2.1. Imaging

We produced an image in the [0.7–1.2] keV band for all the three EPIC detectors (MOS1, MOS2 and pn) using the Extended Source Analysis Software package (ESAS, [Snowden et al. 2008](#)). We used this band as it maximizes the source-to-background ratio for galaxy clusters ([Ettori et al. 2010](#); [Ettori & Molendi 2011](#)), while maintaining a large effective area of the XMM-Newton telescopes. We obtained the count rate map for each EPIC instrument by dividing the raw count image by the exposure maps (tool *exppmap*), accounting for vignetting. The total image, which is shown in Fig. [1](#), was subtracted by the non X-ray background (NXB) image produced by ESAS (tools *mos-spectra*, *pn-spectra*, *mos-back* and *pn-back*), and by the soft-proton contribution as measured within X-COP ([Ghirardini et al. 2018](#)). Point sources were detected down to a fixed flux threshold with the XMM-SAS tool *ewavelet* and excluded using the ESAS task *cheese*. The detailed imaging procedure is described in [Ghirardini et al. \(2019\)](#).

2.2. Spectral analysis

We performed a spectral analysis of the interesting regions following the procedure developed for the X-COP clusters and described in [Ghirardini et al. \(2019\)](#). Here we report the main steps.

Spectra and response files for each region were extracted using the ESAS tasks *mos-spectra* and *pn-spectra* and were fitted using XSPEC v12.9.1 after grouping to ensure a minimum of 20 counts per spectral channel, in the energy band [0.5–10] keV. Point sources detected in the field were always removed before the extraction of the spectra.

We used a detailed modeling of all the various background components to obtain reliable measurements of the physical parameters in regions where the surface brightness barely exceeds the background level. The spectral components for the background are the following: (1) *The non-X-ray Background* (NXB) was estimated for each region from closed-filter observations following the procedure given by [Snowden et al. \(2008\)](#). We left the normalization of the NXB component and those of the prominent background lines free to vary during the fitting procedure, which allows for possible systematic variations of the NXB level. Since all five useful observations were very weakly contaminated by soft proton flares (IN over OUT ratio always ≤ 1.3), we did not include any component to model residual soft protons. (2) *The sky background and foreground components*: we considered the sum of an absorbed power law with a photon index fixed to 1.46, which describes the residual cosmic X-ray background (CXB) ([De Luca & Molendi 2004](#)), an absorbed APEC thermal plasma model with a temperature allowed to vary in the range [0.15 – 0.6] keV, which models the Galactic halo emission ([McCammon et al. 2002](#)), and an unabsorbed APEC model with a temperature fixed to 0.11 keV, which represents the local hot bubble. To estimate the parameters of these sky background components we used a joint analysis of the spectra extracted from the North, East and South observations, in regions at radii larger than R_{200} (~ 1.7 Mpc) from the emission peak of RXCJ1825. These regions are shown in red in Fig. [1](#). (3) Finally, the source is modeled using the thin-plasma emission code *apec* ([Smith et al. 2001](#)), with temperature, metal abundance and normalization as free parameters, and fixed redshift and Galactic column density absorption NH (*phabs* model). We discuss the NH variation in the field of view in Sect. [3.2.1](#).

In the particular case of the detailed spectral study of the temperature and abundance maps in the core regions of RXCJ1825 (Sect. [3.3](#)), we subtracted the background us-

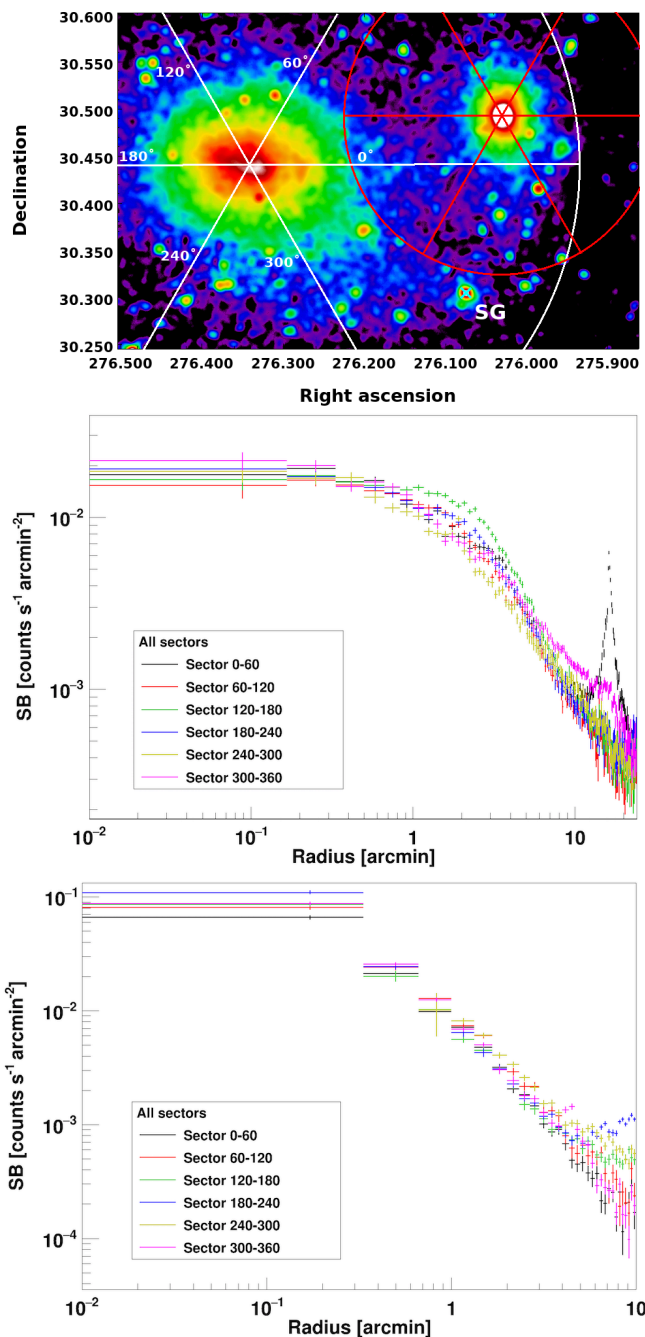


Fig. 2. *Top panel:* Elliptical sectors (60 degrees wide) used for the extraction of surface brightness profiles, overplotted on the XMM-Newton mosaic image (Fig. 1). The orientation angle is calculated counterclockwise from the Right Ascension axis. *Middle panel and bottom panel* show the elliptical surface brightness profiles of RXCJ1825 and CIZAJ1824 extracted in the sectors, respectively. In the x-axis we plot the distances along the major axis of the ellipses. Pointlike sources are removed. The cyan cross shows the position of the Southern Galaxy. The features seen in the profiles are described in Sect. 3.1.1.

ing stacked blank-sky fields following the procedure given in Ghizzardi et al. (2014), and then we extracted the total (source plus background) spectra starting from the soft photon cleaned files produced with ESAS. We preferred to use this method since in this case we decided to extract spectra from polygonal regions (which is not possible with the ESAS software), to better follow the surface brightness

fluctuations present in the core of RXCJ1825. This procedure is fully justified as in the core regions the source is dominant over the background.

3. X-Ray Analysis

In this section we present the results of the X-ray analysis of the extended sources detected in the mosaic image centered on RXCJ1825, including a study of the surface brightness features, temperature and abundance profiles, as well as quantities derived from these profiles. Maps of various thermodynamic quantities for the core of RXCJ1825 and the Southern Galaxy region are also presented.

3.1. X-ray Surface Brightness

3.1.1. Radial profiles in sectors

We first calculated the vignetting-corrected NXB subtracted surface brightness profiles of RXCJ1825 and CIZAJ1824, with the Proffit v.1.5 software (Eckert 2016). We extracted the profiles from a series of concentric elliptical annuli in bins of 10 arcsec (~ 12.5 kpc) along the minor axis, centered on the centroid of the clusters (R.A. = 18h:25m:21.8s, Dec = +30d:26m:25.34s J2000.0 for RXCJ1825, R.A. = 18h:24m:7.1s, Dec = +30d:29m:34.7s for CIZAJ1824); pointlike sources detected in the field have been always removed before the extraction of the profiles.

Fig. 2 shows the surface brightness profiles extracted in six sectors, corresponding to an opening angle of 60 deg (with position angle calculated counterclockwise from the R.A. axis), overplotted on the top of each other.

The profiles of RXCJ1825 (Fig. 2) show large differences between each other, most notably there is an excess surface brightness in the sector with position angle 120-180 deg (green data points), corresponding to a clear asymmetry in the North-East direction for radii smaller than 6 arcmin, whereas sectors 240-300 deg (yellow data) and 300-360 (magenta data) show a clear excess beyond 6 arcmin towards South and South-West, in particular where it is located the Southern Galaxy (SG). The surface brightness peak due to CIZAJ1824 is clearly visible in sectors 0-60 deg (black data) and partially in the 300-360 deg.

Conversely the profiles of CIZAJ1824 (Fig. 2) are remarkably similar up to $\sim 4 - 5$ arcmin. Beyond this radius the scatter increases showing an excess in the three sectors towards RXCJ1825, i.e. 120-180 deg (green), 180-240 deg (blue) and 240-300 deg sectors (yellow). Note that in the 300-360 deg sector (magenta data) there is a peak at ~ 4 arcmin, that is due to a small extended source close to CIZAJ1824 that will be discussed in Sect. 4.3.

3.1.2. Residual and unsharp-mask images

We extracted also the azimuthally averaged (0-360 deg) surface brightness profile for both clusters using concentric elliptical annuli: position angle and ellipticity (i.e. major over minor axis ratio) for the two clusters have been determined using the *proffit - ellipticity* command at $R < 7$ arcmin for RXCJ1825 and $R < 5$ arcmin for CIZA (P.A.=165 deg $\epsilon=1.34$ for RXCJ1825, and P.A.=94 deg, $\epsilon=1.32$ for CIZAJ1824). To avoid the contamination by emission due to the companion cluster, when extracting the profile of